Magneto-electric inversion of a domain pattern

N. Leo,[1,2,*] V. Carolus,[3,*] J. S. White,[4] M. Kenzelmann,[4] M. Hudl,[5] P. Toledano,[6] T. Honda,[7] T. Kimura,[8] S. A. Ivanov,[9] M. Weil,[10] Th. Lottermoser,[1] D. Meier[11] and M. Fiebig[1]

[1]*Department of Materials, ETH Zurich, 8093 Zurich, Switzerland*

[2]*Laboratory for Multiscale Materials Experiments, Paul Scherrer Institut, 5232 Villigen, Switzerland*

[3]*Helmholtz-Institut für Strahlen- und Kernphysik, Universität Bonn, 53115 Bonn, Germany*

[4]*Laboratory for Neutron Scattering and Imaging, Paul Scherrer Institut, 5232 Villigen, Switzerland*

[5]*Department of Physics, Stockholm University, SE-106 91 Stockholm, Sweden*

[6]*Physique des Systèmes Complexes, Université de Picardie, 80.000 Amiens, France*

[7]*Institute of Materials Structure Science, High Energy Accelerator Research Organization (KEK), Tsukuba, Ibaraki 305-0801, Japan*

[8]*Department of Advanced Materials Science, University of Tokyo, 5-1-5 Kashiwanoha, Kashiwa, Chiba 277-8561, Japan*

[9]*Department of Multifunctional Materials, Karpov Institute of Physical Chemistry, Moscow K-64, Russia*

[10]*Institute for Chemical Technology and Analytics, Division of Structural Chemistry, TU Wien, 1060 Vienna, Austria*

[11]*Department of Materials Science and Engineering, Norwegian University of Science and Technology, 7491 Trondheim, Norway*

*These authors contributed equally.

Inversion of an inhomogeneous physical state has great technological significance. For example, active noise reduction has its roots in the emission of an inverted sound wave that interferes destructively with the emitter noise[1]. Inverting the evolution of a spin system by a magnetic-field pulse enables magnetic resonance tomography[2]. In contrast, inversion of a distribution of ferromagnetic or ferroelectric domains is surprisingly difficult. Field poling creates a single-domain state, and piece-by-piece inversion with a scanning tip is impractical. Here we report integral inversion of ferromagnetic or ferroelectric domain patterns in magnetoelectric Co_3TeO_6 and multiferroic Mn_2GeO_4. In either material, an applied field reverses each domain but leaves the domain pattern itself intact. Landau theory reveals this as a general concept where one order parameter holds the memory of the domain structure whereas another one sets its overall sign. Domain pattern inversion is only one example for hidden effects in systems like multiferroics where a multiplicity of complex order parameters are available for combination. Exploring these hidden effects could therefore advance multiferroics to a new level of functionality.

Since their discovery in the 1950s, multiferroics, i.e., materials with a coexistence of magnetic and ferroelectric order, have undergone tremendous development[3,4]. Partly, this is drawn from the desire to control magnetism by electric rather than magnetic fields. Any such magnetoelectric correlation must be permitted by the order and symmetry of the material, however. Particularly complex magnetoelectric couplings may then require the presence of several, often multidimensional order parameters. For example, coexistence of a large magnetization M and

polarization P in hybrid improper ferroelectrics involves three order parameters[5]. Even more are required if $M \,||\, P$ enters as additional condition[6]. It has been little considered that the interplay of so many order parameters is not restricted to merely yielding coupled magnetic and electric order: other valuable properties may emerge — awaiting to be discovered.

Here, we employ the multiplicity of magnetic and electric order parameters to achieve inversion of a ferromagnetic or ferroelectric multi-domain pattern in a single integral step: A homogeneous field reverses the magnetization or polarization of each domain but preserves the original domain pattern. For demonstrating the ubiquitous nature of such holistic inversion, we select two rather different materials, magnetoelectric Co_3TeO_6 and multiferroic Mn_2GeO_4. On these, we demonstrate inversion of a ferromagnetic and a ferroelectric domain pattern, respectively, through imaging of the domain structure by optical second harmonic generation (SHG)[7,8]. Analysis of the free energy reveals that in either compound one order parameter holds the memory of the domain structure whereas another one determines its overall sign. This mechanism is only one example for yet unexplored functionalities hidden in systems with a multitude of complex order parameters.

Co_3TeO_6 forms monoclinic crystals (space group *C2/c1′*). Below 17.7 K, the magnetic order[9–11] is defined by two propagation vectors, $\mathbf{k}_0 = (0,0,0)$ and $\mathbf{k}_{\not 0} \simeq (0,0.5,0.25)$, leading to order parameters $\zeta(\mathbf{k}_0)$ and $\eta(\mathbf{k}_{\not 0})$, respectively (see Methods and Extended Data Fig. 1)[12,13]. The magnetic point group symmetry is $2'$, permitting a spontaneous magnetisation $M_{x,z}(\zeta(\mathbf{k}_0), \eta(\mathbf{k}_{\not 0}))$ and a spontaneous polarisation $P_y(\zeta(\mathbf{k}_0), \eta(\mathbf{k}_{\not 0}))$. Experiments yield $M_{x,z} = 0.57 \cdot 10^{-3}$ μ_B/Co^{2+} but $P_y = 0$[9,10,12].

Mn_2GeO_4 forms orthorhombic crystals (space group $Pnma1'$). The multiferroic phase below 5.5 K is characterised by four magnetic order parameters associated with the co-existing magnetic propagation vectors $\mathbf{k}_0 = (0,0,0)$ and $\mathbf{k}_{\not 0} = (\pm 0.136, \pm 0.211, 0)$. Two order parameters, $X_1(\mathbf{k}_0)$ and $X_3(\mathbf{k}_0)$, describe commensurate antiferromagnetic and ferromagnetic contributions, respectively, while two others, $\mathrm{M}^{\mathrm{D1}}(\mathbf{k}_{\not 0})$ and $\mathrm{M}^{\mathrm{D2}}(\mathbf{k}_{\not 0})$, describe incommensurate spiral components[6,14,15]. The magnetic point group symmetry is *2* and a spontaneous magnetization $M_z \propto X_3(\mathbf{k}_0)$ and a magnetically induced electric polarization $P_z \propto \mathrm{M}^{\mathrm{D1,2}}(\mathbf{k}_{\not 0})$ coexist (see Methods and Extended Data Fig. 2). Experiments yield[6,16] $M_z = 7 \cdot 10^{-3}$ $\mu_\mathrm{B}/\mathrm{Mn}^{2+}$ and $P_z = 6$ $\mu\mathrm{C\,m}^{-2}$.

We image the spatial distributions of domains by SHG — frequency doubling of light in a material[7]. The relation between the polarizations of the incident and emitted light at frequencies ω and 2ω, respectively, depends on the symmetry of the material. As any type of ferroic order changes the point group symmetry, characteristic SHG contributions emerge that allow to image the associated domain patterns[8] with a resolution of about 1 μm. In particular, SHG detects the small spontaneous magnetization or polarization that is often associated with multiferroic materials (see Methods for details on the SHG coupling and experiment)[4].

SHG spectra from a z-oriented Co_3TeO_6 platelet (Fig. 1a) yield maxima at 2.56 eV and 2.65 eV from electronic transitions within the $\mathrm{Co}^{2+}(3d)$ band. The polarization of the SHG light and its presence below 17.4 K only (Fig. 1b) are in line with coupling to $M_{x,z}$ (see Methods). We use this SHG signal to image the ferromagnetic $M_{x,z}$ domain distribution in a zero-field-cooled z-oriented Co_3TeO_6 sample. Interference with a crystallographic SHG background signal reveals

domains at $+M_{x,z}$ and $-M_{x,z}$ as regions of different brightness in Fig. 1c (see Methods).

Figure 2 shows the evolution of a $M_{x,z}$ domain structure for a magnetic field $\mu_0 H_y$ swept across the ± 2.4 T range. Because of $H_y \perp M_{x,z}$, the field does not convert the $\pm M_{x,z}$ domains into a single-domain state. Zero-field cooling reveals a multitude of domains, while application of $+2.4$ T yields a simplified pattern with few dominant domains (Fig. 2b). When the field is reversed, the number of domains increases around 0 T (Fig. 2c). At -2.4 T, however, we obtain a domain pattern that is nearly identical to the state at $+2.4$ T (Fig. 2a), but with an inverted brightness of each domain (Fig. 2d). Apparently, $M_{x,z}$ is reversed in each individual domain, yet without affecting shape and distribution of the domains as such. We thus find a striking integral inversion of an inhomogeneous distribution of ferromagnetic domains by a homogeneous field.

Note that the reversal occurs via intermittent formation and shifts of domain walls (Fig. 2c). This and the H_y-independence of the magnitude of $M_{x,z}$ (see Fig. 1d) rule out that the brightness inversion is an optical artefact. Furthermore, the domain-wall mobility excludes that the protection of the domain pattern is caused by pinning effects. According to the magnetic-field dependence of the SHG interference in Fig. 2e, integrated in a sweep in the ± 3 T range over two spots of ~ 500 μm, the most significant domain variations occur in the ± 0.2 T range. The surprising protection of the domain pattern at high fields is in stark contrast to its variability at low fields.

The inversion of the $M_{x,z}$ domain pattern by the homogeneous H_y field is resolved by a free-energy term coupling $M_{x,z}(\zeta(\mathbf{k}_0), \eta(\mathbf{k}_\emptyset))$ to H_y in a sign-sensitive way. An analysis of Landau

invariants reveals the lowest-order term enabling such coupling as

$$F_{\mathrm{inv}} \propto \mathscr{C}\left(\mathbf{k}_{\emptyset}\right) \cdot M_y(H_y) \cdot M_{x,z}. \tag{1}$$

Here, $\mathscr{C}(\mathbf{k}_{\emptyset})$ is a product of the components of $\eta(\mathbf{k}_{\emptyset})$ that establishes the invariance of the free-energy contribution F_{inv} (see Methods for its derivation)[17]. Since a magnetic field H_y induces a proportional magnetization M_y and does not act on $\mathscr{C}(\mathbf{k}_{\emptyset})$, a reversal of $H_y \propto M_y$ entails reorientation of $M_{x,z}$ to retain $F_{\mathrm{inv}} < 0$ for ground-state energy minimization. This sensitivity of the *orientation* of $M_{x,z}$ to H_y does not contradict the aforementioned near-insensitivity of the *magnitude* of $M_{x,z}$ to H_y as these originate from different coupling terms. Hence, the same order parameters responsible for magnetoelectric coupling in Co_3TeO_6 provide the basis for other intriguing cross-correlations, here the integral inversion of a ferromagnetic domain pattern.

To support our claim of generality for the domain-inversion behaviour, we now turn towards Mn_2GeO_4, a material differing from Co_3TeO_6 in crystal structure as well as magnetic and electric order.

The SHG spectrum of a z-oriented Mn_2GeO_4 platelet (Fig. 3a) yields a peak at 1.83 eV. The signal is present in the multiferroic phase below 5.5 K only (Fig. 3b), implying coupling to M_z or P_z. Zero-field cooling resolves a multitude of domains and domain walls (Fig. 3c), but application of an electric field $E_z = 144$ kV cm^{-1} transforms this into a single-domain state (Fig. 3d). In contrast, a magnetic field H_z above the coercive field leaves the sample in a multi-domain state (Fig. 4a). Therefore we conclude that SHG couples to the spontaneous polarisation P_z but not to the magnetization M_z.

The evolution of the ferroelectric P_z domains with an applied magnetic field H_z is shown in Fig. 4. First, the sample is field-cooled at $H_z = -230$ mT which induces a single-domain $-M_z$ state[6] but, according to the SHG image at $H_z = 0$ in Fig. 4a, retains a ferroelectric multi-domain state. As H_z is increased towards positive values, additional ferroelectric domain walls are formed and move across the sample. At $+150$ mT we obtain a ferroelectric domain pattern nearly identical to the one observed initially, except that P_z in each domain is reversed (Fig. 4h). Increasing H_z yields no additional change, and further field cycles corroborate the reproducibility of the local P_z inversion without changes to the domain pattern.

We thus encounter a situation for the ferroelectric order in Mn_2GeO_4 that is analogous to the ferromagnetic order of Co_3TeO_6. The order parameter of each domain is reversed, but the domain pattern as such is left untouched, a phenomenon beyond the magnetoelectric switching between single-domain states discussed so far[6,18]. To explain the domain inversion in Mn_2GeO_4, we require a sign-sensitive coupling between P_z and H_z. An analysis of Landau invariants involving the order parameters $X_{1,3}(\mathbf{k}_0)$ and $\mathrm{M}^{\mathrm{D}1,2}(\mathbf{k}_{\emptyset})$ reveals

$$F_{\mathrm{inv}} \propto \mathscr{C}(\mathbf{k}_0) \cdot M_z(H_z) \cdot P_z \tag{2}$$

with $\mathscr{C}(\mathbf{k}_0) \propto X_1(\mathbf{k}_0)$ (see Methods)[14,15]. Cooling in a magnetic field H_z sets a uniform magnetization $M_z \propto H_z$. This still allows a $\pm P_z$ domain distribution because $F_{\mathrm{inv}} < 0$ can be retained by the sign of $\mathscr{C}(\mathbf{k}_0)$. As $\mathscr{C}(\mathbf{k}_0)$ remains invariant under application of H_z, the free energy is minimised only if P_z switches simultaneously with the reversal of $M_z \propto H_z$.

Thus, in two different materials we have demonstrated the inversion of ferromagnetic or

ferroelectric domain patterns with a single sweep of a homogeneous, non-conjugated field. In each domain, the local order parameter is reversed, but the domain pattern itself is left untouched. In a generalization of our two examples, Co_3TeO_6 and Mn_2GeO_4, we can express the inversion by a trilinear coupling term in the free energy:

$$F_{\mathrm{inv}} \propto \hat{I} \cdot \hat{S}(H_S) \cdot \hat{O} \tag{3}$$

The effect of this coupling term is illustrated in Fig. 5. $\hat{O}$ represents the experimentally observed domain distribution, i.e., magnetization or polarization. The term $\hat{I}$ contains the memory of the domain pattern that is preserved, as it remains invariant under the applied field H_S. In contrast, $\hat{S} \equiv \hat{S}(H_S)$ can be switched by H_S. At $H_S \ll 0$, $\hat{S}$ is in a single-domain -1 state and the observable $\hat{O}$ assumes the domain structure of $\hat{I}$. When crossing $H_S = 0$, $\hat{S}$ becomes transiently multi-domain; consequently, new domain walls appear in $\hat{O}$ and propagate across the sample. At $H_S \gg 0$, $\hat{S}$ resumes the single-domain state (now $+1$) and the initial domain configuration of $\hat{I}$ is recovered in $\hat{O}$, albeit with reversed orientation of $\hat{O}$ in each domain because of the H_S-controlled sign change of $\hat{S}$. The deterministic interchange of domain patterns expressed by Eq. (3) distinguishes our experiment from the non-deterministic switching between multidomain patterns found, e.g., in partial ferroics[19]. The expressions for $\hat{I}$, $\hat{S}$ and $\hat{O}$ are sample-specific (see Tab. 1 and Methods), but supported by the independence of our two chosen examples, Co_3TeO_6 and Mn_2GeO_4, we argue that the inherent complexity of a system characterized by several multidimensional order parameters at different magnetic propagation vectors $\mathbf{k}$ renders their widespread existence and coupling likely.

Multiferroics are ideal for integral domain inversion because of the order-parameter com-

plexity required to achieve strongly coupled magnetic and electric order. $CoCr_2O_4$ or, at room temperature, hexaferrites may be candidates[18,20–22]. Aside from symmetry, material parameters need to be satisfied. Coupling between $\hat{I}$ and $\hat{S}$ beyond that in Eq. (3) (like by strain) must be small. Furthermore, the $\hat{I}$ walls must not pin the motion of the $\hat{S}$ walls during the inversion. On the other hand, a domain inversion mechanism alternative to the one presented by us may entirely root in domain-wall coupling and be absent within the domains. $GdFeO_3$ or the hexagonal manganites are possible candidates[18,23]. This reconfirms that we presented just one out of many conceivable examples for order-parameter coupling beyond mere magnetoelectric phase control. A realm of other multi-order-parameter functionalities remains to be explored.

1. Hansen, C. H., *Understanding Active Noise Cancelation* (Spon Press, New York, 2001).

2. Jung, B. A. & Weigel, M. Spin echo magnetic resonance imaging. *J. Magn. Reson. Imaging* **37,** 805-817 (2013).

3. Wang, K. F., Liuab, J.-M. & Renc, Z. F. Multiferroicity: the coupling between magnetic and polarization orders. *Adv. Phys.* **58,** 321-448 (2009).

4. Fiebig, M., Lottermoser, Th., Meier, M. & Trassin, M. The evolution of multiferroics. *Nature Rev. Mater.* **1,** 16046 (2016).

5. Benedek, N. A., & Fennie, C. J. Hybrid improper ferroelectricity: a mechanism for controllable polarization-magnetization coupling. *Phys. Rev. Lett.* **106,** 107204 (2011).

6. White, J. S. *et al.* Coupling of magnetic and ferroelectric hysteresis by a multicomponent magnetic structure in Mn_2GeO_4. *Phys. Rev. Lett.* **108,** 077204 (2012).

7. Pershan, P. S. Nonlinear optical properties of solids: energy considerations. *Phys. Rev.* **130,** 919 (1963).

8. Fiebig, M., Pavlov, V. V. & Pisarev, R. V. Second-harmonic generation as a tool for studying electronic and magnetic structures of crystals. *J. Opt. Soc. Am. B* **22,** 96-118 (2005).

9. Singh, H., Ghosh, H., Chandrasekhar Rao, T. V., Sharma, G., Saha, J. & Patnaik, S. Short range ferromagnetic, magneto-electric, and magneto-dielectric effect in ceramic Co_3TeO_6. *J. Appl. Phys.* **119,** 044104 (2016).

10. Hudl, M. *et al.* Complex magnetism and magnetic-field-driven electrical polarization in Co_3TeO_6. *Phys. Rev. B* **84,** 180404 (2011).

11. Li, W.-H., Wang, C.-W., Hsu, D., Lee, C.-H., Wu, C.-M., Chou, C.-C., Yang, H.-D., Zhao, Y., Chang, S., Lynn, J.-W. & Berger, H. Interplay between the magnetic and electric degrees of freedom in multiferroic Co_3TeO_6. *Phys. Rev. B* **85,** 094431 (2012).

12. Tolédano, P. *et al.* First-order multi-k phase transitions and magnetoelectric effects in multiferroic Co_3TeO_6. *Phys. Rev. B* **85,** 214439 (2012).

13. Ivanov, S. A., Tellgren, R., Ritter, C., Nordblad, P., Mathieu, R., André, G., Golubko, N. V., Politova, E. D. & Weil, M. Temperature-dependent multi-k magnetic structure in multiferroic Co_3TeO_6. *Mat. Res. Bull.* **47,** 63 (2012).

14. Honda, T. *et al.* Coupled multiferroic domain switching in the canted conical spin spiral system Mn_2GeO_4. *Nat. Commun.* **8,** 14457 (2017).

15. Harris, A. B. Identifying Landau order parameters and their transformation properties for complex multiferroics: The case of Mn_2GeO_4. *Phys. Rev. B* **96,** 054422 (2017).

16. Honda, T., Ishiguro, Y., Nakamura, H., Wakabayashi, Y. & Kimura, T. Structure and magnetic phase diagrams of multiferroic Mn_2GeO_4. *J. Phys. Soc. Jpn.* **81,** 103703 (2012).

17. Carolus, V. *Topography and Manipulation of Magnetic Domains in Cobalt Tellurite* (PhD thesis, Bonn, 2014).

18. Tokunaga, Y., Furukawa, N., Sakai, H., Taguchi, Y., Arima, T.-H. & Tokura, Y. Composite domain walls in a multiferroic perovskite ferrite. *Nat. Mater.* **8,** 558-562 (2009).

19. Aizu K. Possible species of ferromagnetic, ferroelectric, and ferroelastic crystals. *Phys. Rev. B* **2,** 754 (1970).

20. Yamasaki, Y., Miyasaka, S., Kaneko, Y., He, J.-P., Arima, T. & Tokura, Y. Magnetic reversal of the ferroelectric polarization in a multiferroic spinel oxide. *Phys. Rev. Lett.* **96,** 207204 (2006).

21. Tokunaga, Y., Kaneko, Y., Okuyama, D., Ishiwata, S., Arima, T., Wakimoto, S., Kakurai, K., Taguchi, Y. & Tokura, Y. Multiferroic M-type hexaferrites with a room-temperature conical state and magnetically controllable spin helicity. *Phys. Rev. Lett.* **105,** 257201 (2010).

22. Zhai, K., Wu, Y., Shen, S., Tian, W., Cao, H., Chai, Y., Chakoumkos, B. C., Shang, D., Yan, L., Wang, F. & Sun, Y. Giant magnetoelectric effects achieved by tuning spin cone symmetry in Y-type hexaferrites. *Nat. Commun.* bf 8, 51 (2017).

23. Fiebig, M., Lottermoser, Th., Fröhlich, D., Goltsev, A. V. & Pisarev, R. V. Observation of coupled magnetic and electric domains. *Nature* **419,**, 818 (2002).

Acknowledgements J. S. W. thanks the SNSF for support via the grant 200021_153451. M. K. acknowledges financial support by the SNSF grant 200021_165855. Financial support of this research from the Russian Foundation for Basic Research is gratefully acknowledged by S. A. I.

Author Contributions All authors contributed to the discussion and interpretation of the experiment and to the completion of the manuscript. N. L. and V. C. performed the experiments. N. L, J. S. W. and M. K. developed a comprehensive Landau-theoretical description of the domain inversion. V. C., M. H. and P. T. performed the Landau-theoretical analysis of the Co_3TeO_6 experiments. M. W. grew single crystals of Co_3TeO_6 and S. A. I. analyzed their stoechiometry and structure. T. H. and T. K. prepared single crystals of Mn_2GeO_4. T. L. supervised the experiments on Co_3TeO_6. D. M. and M. F. initiated the experiment and supervised the work.

Competing Interests The authors declare that they have no competing financial interests.

Correspondence Correspondence and requests for materials should be addressed to M. F. (email: manfred.fiebig@mat.ethz.ch).

	$\hat{I}$	$\hat{S}(H_S)$	$\hat{O}$
Co_3TeO_6	$\mathscr{C}\left(\mathbf{k}_{\not\emptyset}\right) \mapsto \eta$	$M_y(H_y) \mapsto \zeta$	$M_{x,z} \mapsto \eta, \zeta$
Mn_2GeO_4	$\mathscr{C}\left(\mathbf{k}_0\right) \mapsto X_1$	$M_z(H_z) \mapsto X_3$	$P_z \mapsto X_1, X_3$

Table 1: **Material-specific terms, switching fields, observables, and their relation to the order parameters.** Values of the terms $\hat{I}$, $\hat{S}(H_S)$ and $\hat{O}$ in Eqs. (1) and (2) and their dependence on, respectively coupling to the order parameters of Co_3TeO_6 and Mn_2GeO_4. See Methods for the explicit definitions of order parameters and of $\hat{I}$, $\hat{S}$, and $\hat{O}$.

Figure 1: **Probing ferromagnetism in Co_3TeO_6 by SHG. a**, SHG intensity spectrum at 5 K for x-polarized frequency-doubled and y-polarized incident light ($\sim \chi_{xyy}$). Henceforth, photon energies at the intensity maxima at 2.56 eV and 2.65 eV are used. **b**, Temperature dependence of the χ_{xyy}-related SHG intensity. The signal is observed in the magnetoelectric phase below 17.4 K only. **c**, Distribution of ferromagnetic domains in a z-oriented Co_3TeO_6 sample. A SHG interference technique visualizes the $\pm M_{x,z}$ domains as regions with different brightness (see Methods and Extended Data Fig. 3). The scale bar measures 500 μm. **d**, Weak dependence of the χ_{xyy}-related SHG intensity on a magnetic field H_y. In contrast to **c**, the SHG yield is independent of the domain state because the SHG interference technique generating the contrast between opposite domain states in **c** is not applied. Thus, unperturbed by the domain state, **d** reveals the H_y dependence of the magnitude of $M_{x,z}$.

Figure 2: **Inversion of ferromagnetic domain pattern in Co_3TeO_6. a-d**, Sequentially taken SHG images of the $\pm M_{x,z}$ domain pattern on a z-oriented Co_3TeO_6 sample at the given magnetic fields H_y. The scale bar measures 500 μm. **e**, Dependence of the $M_{x,z}$ domain state on a magnetic field H_y. The domain-state-sensitive SHG interference (see Methods) was measured on two spots of 500 μm diameter lying outside the area shown in **a**-**d**. Tuning the magnetic field between positive to negative values reverses the magnetization of each domain while the domain pattern as such is left intact. The interchange is mainly limited to the field interval ± 0.2 T. The inversion progresses via transient formation and shifts of domains and domain walls.

Figure 3: **Probing ferroelectricity in Mn_2GeO_4 by SHG. a**, SHG intensity spectrum at 4.4 K for z-polarised frequency-doubled and y-polarised incident light ($\sim \chi_{zyy}$). The peak at 1.83 eV identifies the photon energy chosen for the following measurements. **b**, Temperature dependence of the χ_{zyy}-related SHG intensity after subtraction of temperature-independent background contributions from the surface and higher-order-multipole SHG. A signal is observed in the multiferroic phase below 5.5 K only. **c**, The domain structure of a zero-field-cooled sample reveals an inhomogeneous distribution of bright and dark regions, indicating a large number of domains and domain walls. The scale bar measures 500 μm **d**, After application of an electric field $E_z = 144$ kVcm^{-1} the SHG image assumes homogeneous brightness, indicating a ferroelectric single-domain state, in the region where the transparent electrodes overlap (white outline).

Figure 4: **Inversion of ferroelectric domain pattern in Mn_2GeO_4.** Sequentially taken SHG images of $\pm P_z$ domains on a z-oriented Mn_2GeO_4 sample at given magnetic fields H_z (see Extended Data Fig. 4 for the corresponding experiment on a x-oriented sample). Because of the small SHG contrast, domain states at $+P_z$ and $-P_z$ are highlighted by colour shading. **a**, After field-cooling at $H_z = -230$ mT, followed by setting $H_z = 0$, the sample is in a ferroelectric multi-domain state. **b-g**, Application of $H_z > 0$ leads to additional nucleation and movement of domain walls. **h**, In the saturated state at $+150$ mT, however, almost the same domain distribution as after the original field cooling in **a** is obtained, yet with reversed orientation of the ferroelectric polarization in each domain.

Figure 5: **Multi-order-parameter model for integral domain inversion.** $\hat{O}$ represents the domain distribution observed in the experiment, i.e., magnetization for Co_3TeO_6 or polarization for Mn_2GeO_4. $\hat{I}$ contains the memory of the domain pattern to be preserved in $\hat{O}$. $\hat{S} \equiv \hat{S}(H_S)$ is switched between a uniform -1 and a uniform $+1$ state by ramping the applied field H_S between its negative and positive maximum values. Reversal of $\hat{S}$ by H_S entails reversal of $\hat{O}$ in order to minimize the free energy in Eq. (3), since $\hat{I}$ itself is immutable under H_S. Thus, the field H_S reverses the orientation of the order parameter of $\hat{O}$ in each domain, but preserves the domain structure. When crossing $H_S = 0$, $\hat{S}$ enters a transient multi-domain state with the nucleation and propagation of $(-1)/(+1)$ domain walls. This leads to the observed transient increase in the number of domain walls and their propagation in $\hat{O}$. The sample-specific expressions for $\hat{I}$, $\hat{S}$ and $\hat{O}$ are listed in Table 1.

Methods

Sample preparation. Single-crystals of Co_3TeO_6 were grown by the chemical vapour transport method. The chemical composition and the homogeneity of the crystals were analyzed by energy-dispersive spectroscopy using a JEOL 840A scanning electron microscope and INCA 4.07 (Oxford Instruments) software. For the sample prepared for diffraction measurements the cation content was also determined by inductively coupled plasma atomic emission spectroscopy performed with an ARL Fisions 3410 spectrometer. According to the elemental analysis done on 20 different crystallites, the stoechiometry is $Co_{2.98(3)}$, $Te_{1.02(3)}$ and $O_{5.99(2)}$ (oxygen value derived by iodometric titration). Room-temperature X-ray diffraction pattern on a Bruker D8 Advance diffractometer yielded $a = 14.8117(4)$ Å, $b = 8.8392(3)$ Å, $c = 10.3587(4)$ Å, $\beta = 94.84(1)^\circ$ as monoclinic unit-cell parameters. Single-crystals of Mn_2GeO_4 were grown by the floating-zone method as described elsewhere[13,16]. All crystals were oriented by Laue diffraction, cut, lapped to a thickness of about 50 μm and polished from both sides with silica slurry.

Second harmonic generation (SHG). SHG denotes doubling of the frequency of a light wave in a material. Restricting ourselves to the (leading) electric-dipole approximation, this is described by[7] $P_i(2\omega) \propto \chi_{ijk} E_j(\omega) E_k(\omega)$. Here, $E_{j,k}(\omega)$ denote the electric-field components of the incident light and $P_i(2\omega)$ is the induced i-polarized nonlinear polarization acting as source for the emitted SHG wave at intensity $I \propto |\mathbf{P}(2\omega)|^2$. The nonlinear susceptibility tensor $\hat{\chi}$ characterizes the symmetry of the host material[24]. As ferroic order changes the point group symmetry, it will lead to the emergence of ordering-induced contributions to the SHG yield that we employ for probing this order with spectral and spatial resolution[8]. Domain states with opposite orientation of the order

parameter differ in the sign of the corresponding SHG light waves, equivalent to a 180° phase shift. This allows to image opposite domain states as regions of different brightness via an interference technique[25] illustrated in Extended Data Fig. 3. The detailed setup for transmission SHG experiments is described elsewhere[8].

SHG experiments on Co_3TeO_6. The magnetic point group symmetry $2'$ of the phase below 17.4 K permits a set of time-reversal-symmetry-violating ("c-type") electric-dipole SHG contributions proportional to $M_{x,z}$. According to symmetry tables[24], this set includes 14 tensor components. We observed all of these and verified that they display the same $M_{x,z}$-related temperature dependence as in Fig. 1b. In turn, no other tensor components yielding an order parameter coupling were identified, in consistence with the $2'$ point group symmetry and the earlier observation that P_y, though allowed, is measured as zero[9,10,12]. According to theory, the coupling to the magnetic order parameter by SHG is typically the result of the low-symmetry environment of the paramagnetic ions in combination with spin-orbit interaction[8]. Experiments were performed in a liquid-helium-operated split-coil magnetic-field cryostat on a z-cut sample with light in perpendicular incidence. We used light pulses of 5 ns emitted from an optical parametric oscillator pumped by the frequency-tripled light emitted from a Nd:YAG laser. Superposition of the SHG wave from the χ_{xyy} component with a constant crystallographic SHG reference contribution from the χ_{yyy} component is used for the aforementioned interference technique identifying opposite domain states by their different brightness[25].

SHG experiments on Mn_2GeO_4. The point group symmetry 2 of the multiferroic phase below 5.5 K allows a set of time-reversal-symmetry-conserving ("i-type") electric-dipole SHG contribu-

tions proportional to P_z. This set includes 13 components[24] from which we selected χ_{zyy} and χ_{yyz}. Experiments were performed on a z-cut sample onto which transparent electrodes were sputtered for applying large electric fields. In order to access the z-polarized SHG contribution in χ_{zyy}, the sample was tilted with respect to the direction of the incident light. In addition, we show experiments for χ_{yyz} on a x-cut sample as Extended Data Fig. 4. We used light pulses of 120 fs emitted from an optical parametric amplifier pumped by an amplified Ti:sapphire laser system. Destructive interference of SHG waves from opposite $\pm P_z$ domain states at the position of the domain walls reveals the domain boundaries as black lines meandering through the SHG image[26]. These are used to identify the ferroelectric domain pattern.

Landau theory on the low-temperature phase of Co_3TeO_6. Here we provide the link between the qualitative treatment of the propagation vectors, order parameters and invariants describing the magnetoelectric order of Co_3TeO_6 in the main text and the full group-theoretical derivation. Please also refer to Refs. 12 and 17 for the latter. Using the notation of Ref. 12, the phase of Co_3TeO_6 below 17.4 K is characterised by two magnetic order parameters associated with the co-existing magnetic modulations vectors $\mathbf{k}_0 \equiv \mathbf{k}_2 = (0,0,0)$ and $\mathbf{k}_{\emptyset} \equiv \mathbf{k}_3 \simeq (0,0.5,0.25)$[13]. $\mathbf{k}_0$ is associated with the one-dimensional magnetic order parameter $\zeta(\mathbf{k}_0)$, and from the one-dimensional little group of the four-armed star of $\mathbf{k}_{\emptyset}$ one can construct the four-dimensional order parameter $\eta(\mathbf{k}_{\emptyset}) = (\rho_1 e^{i\theta_1}, \rho_1 e^{-i\theta_1}, \rho_2 e^{i\theta_2}, \rho_2 e^{-i\theta_2})$[12]. The latter is simplified by $\rho_1 = \rho_2 \equiv \rho_e$ and $\theta_1 = \theta_2 \equiv \theta_e$ because of the (approximate[11]) commensurability of $\mathbf{k}_{\emptyset}$. The coexisting antiferromagnetic order parameters $\zeta(\mathbf{k}_0)$ and $\eta(\mathbf{k}_{\emptyset})$ yield the magnetic point group symmetry $2'$ which permits a spontaneous magnetisation $M_{x,z} \propto \zeta\rho_e^4 \cos 4\theta_e$ and a spontaneous electric polarisation

$P_y \propto \zeta^2 \rho_e^4 \cos 4\theta_e$. The latter was not detected at zero magnetic field, however, rendering Co_3TeO_6 a magnetoelectric rather than a multiferroic compound[10,12].

To explain the inversion of the $M_{x,z}$ domains under application of a magnetic field H_y, we require a coupling connecting $M_{x,z}(\zeta(\mathbf{k}_0), \eta(\mathbf{k}_\emptyset))$ and $M_y(H_y)$ in a sign-sensitive way that complies with the invariance of the free energy under the symmetry operations of the parent phase. In particular, translational invariance poses a rather restrictive constraint: For order parameters at incommensurate propagation vectors, here $\mathbf{k}_\emptyset$, translational invariance can be retained only if these order parameters enter the free energy in even powers. The even power, however, preserves time reversal symmetry so that another — time-reversal-symmetry-violating — order parameter associated to a commensurate propagation vector, here $\mathbf{k}_0$, has to enter the trilinear term in Eq. (1).

Using the transformation behaviour of the order parameters $\eta(\mathbf{k}_\emptyset)$ and $\zeta(\mathbf{k}_0)$, described by the irreducible representations $\tau_1(\mathbf{k}_\emptyset)$ and $\Gamma_4(\mathbf{k}_0)$, respectively, from Ref. 12, we then find $F_{\text{inv}} \propto \sigma_4(\mathbf{k}_\emptyset)\zeta(\mathbf{k}_0)M_y(H_y)$ as simplest coupling term to the free energy. Here, $\sigma_4(\mathbf{k}_\emptyset) = (\rho_1^4 \sin 4\theta_1 - \rho_2^4 \sin 4\theta_2)$ is a forth-order product of the elements of $\eta(\mathbf{k}_\emptyset)$, which transforms like the irreducible representation $\tau_1(\mathbf{k}_\emptyset)$ and retains the invariance of F_{inv}. Because of $M_{x,z} \propto \zeta(\mathbf{k}_0)$, we have thus reconstructed the expression in Eq. (1), finding $\mathscr{C}\left(\mathbf{k}_\emptyset\right) = \frac{\sigma_4}{\rho_e^4 \cos 4\theta_e}$. Note that $\sigma_4(\mathbf{k}_\emptyset)$ is non-zero only if $\mathbf{k}_\emptyset$ is incommensurate so that the degeneracy of ρ_e and θ_e is lifted (i.e. $\rho_1 \neq \rho_2$ and $\theta_1 \neq \theta_2$). A small incommensurate modulation was indeed observed[11] in Co_3TeO_6 but usually is neglected because of the smallness of this correction[12]. In the domain-inversion mechanism, however, it generates the leading-order coupling term.

Landau theory on the multiferroic phase of Mn_2GeO_4. Here we provide the link between the qualitative treatment of the propagation vectors, order parameters and invariants describing the magnetoelectric order of Mn_2GeO_4 in the main text and the full group-theoretical derivation. Please also refer to Refs. 14 and 15 for the latter. Using the notation of Refs. 14 and 15, the multiferroic phase of Mn_2GeO_4 below 5.5 K is characterised by four magnetic order parameters associated with the co-existing magnetic modulation vectors $\mathbf{k}_0 \equiv \mathbf{Q}_c = (0,0,0)$ and $\mathbf{k}_{\emptyset} \equiv \mathbf{Q}_{ic} = (\pm 0.136, \pm 0.211, 0)$. The two one-dimensional order parameters related to $\mathbf{k}_0$ are X_1 and X_3. From the two-dimensional little group of the four-armed star of $\mathbf{k}_{\emptyset}$ one can construct two four-dimensional magnetic order parameters $\mathrm{M}_{\mathrm{Q}}^{\mathrm{D1}}$ and $\mathrm{M}_{\mathrm{Q}}^{\mathrm{D2}}$ with $\mathrm{M}_{\mathrm{Q}}^{\mathrm{D}i} = (\mathrm{M}_{\mathrm{QA}}^{\mathrm{D}i}, \mathrm{M}_{\mathrm{QB}}^{\mathrm{D}i}, \mathrm{M}_{\mathrm{QA}}^{\mathrm{D}i^*}, \mathrm{M}_{\mathrm{QB}}^{\mathrm{D}i^*})$ and $i = 1,2$. Here A and B refer to the two possible directions of the magnetic propagation vector $\mathbf{k}_{\emptyset}$. The corresponding magnetic point group[6,14–16] is *2*. Antiferromagnetic components $\propto X_1(\mathbf{k}_0)$ and a spontaneous magnetization $M_z \propto X_3(\mathbf{k}_0)$ coexist with a spontaneous electric polarisation $P_z \propto \mathrm{A_{ic}} - \mathrm{B_{ic}}$ so that $P_z \parallel M_z$ (corresponding to the term U in Refs. 14 and 15). Here, $J_{\mathrm{ic}} = \mathrm{M}_{\mathrm{QJ}}^{\mathrm{D1}}\mathrm{M}_{\mathrm{QJ}}^{\mathrm{D2}*} - \mathrm{M}_{\mathrm{QJ}}^{\mathrm{D1}*}\mathrm{M}_{\mathrm{QJ}}^{\mathrm{D2}}$ for $J = \mathrm{A}, \mathrm{B}$.

For the domain inversion, a sign-sensitive coupling of $P_z(\mathbf{k}_{\emptyset})$ to H_z, respectively $M_z(H_z)(\mathbf{k}_0)$, is required. The lowest-order contribution permitting this is $F_{\mathrm{inv}} \propto X_1 X_3(\mathrm{A}_{\mathrm{ic}}^2 - \mathrm{B}_{\mathrm{ic}}^2) \propto X_1(\mathrm{A_{ic}} + \mathrm{B_{ic}}) M_z P_z$. This reconstructs the expression in Eq. (2), yielding $\mathscr{C}(\mathbf{k}_0) = X_1(A_{\mathrm{ic}} + B_{\mathrm{ic}})$, and corresponds to the term W in Refs. 14 and 15. Note that $\mathscr{C}(\mathbf{k}_0)$ contains contributions associated with both $\mathbf{k}_0$ as well as $\mathbf{k}_{\emptyset}$. The term $(A_{\mathrm{ic}} + B_{\mathrm{ic}}) \sim \mathbf{k}_{\emptyset}$, however, merely retains the correct symmetry of the coupling, while $X_1(\mathbf{k}_0)$ holds the domain structure that determines the parallel or antiparallel orientation of M_z and P_z such that $F_{\mathrm{inv}} < 0$ (Refs. 14, 15). Reversal of the field H_z reverses the

magnetisation M_z. Microscopically, this swaps the orientation of the Mn^{2+} spin cones (see Extended Data Fig. 2), corresponding to an exchange of A_{ic} and B_{ic}. Because of $P_z \propto A_{ic} - B_{ic}$, this simultaneously reverses the direction of polarization [14,15].

24. Birss, R. R. *Symmetry and Magnetism* (North-Holland, Amsterdam, 1966).

25. Leute, S., Lottermoser, Th. & Fröhlich, D. Nonlinear spatially resolved phase spectroscopy. *Opt. Lett.* **24,** 1520–1522 (1999).

26. Fiebig, M., Fröhlich, D., Lottermoser, Th., & Maat, M. Probing of ferroelectric surface and bulk domains in ferroelectric RMnO$_3$ (R = Y, Ho) by second harmonic generation, *Phys. Rev. B* **66,** 144102 (2002).

Data availability The data that support the findings of this study are available from the corresponding author upon reasonable request.

Extended Data Figure 1: **Co_3TeO_6 — crystallographic structure, magnetic structure and optical excitation.** **a**, Three-dimensional view of the crystallographic unit cell along the x axis in relation to magnetic propagation vectors $\mathbf{k}_0$ and $\mathbf{k}_{\not 0}$. **b**, Section of the unit cell in the xz plane showing the location of the paramagnetic Co^{2+} ions on its five different positions. **c**, Magnetic moments of the Co^{2+} ions shown in **b**. **d**, Orientation of the spontaneous magnetization $M_{x,z}$ and the electric polarization P_y. The latter is symmetry-allowed as spontaneous polarization, yet only observed as magnetic-field induced contribution[9,10,12]. **e**, Geometry of the SHG transmission experiment with light at ω and 2ω propagating along the z axis, probing a z-cut Co_3TeO_6 platelet in perpendicular incidence. The sample is exposed to a magnetic field H_y.

Extended Data Figure 2: **Mn_2GeO_4 — crystallographic structure, magnetic structure and optical excitation.** **a**, Top: three-dimensional view of the crystallographic unit cell showing the location of the paramagnetic Mn^{2+} ions on the different positions Mn1 and Mn2. Bottom: orientation of the spontaneous magnetization M_z and spontaneous polarization P_z in relation to the magnetic propagation vectors $\mathbf{k}_0$ and $\mathbf{k}_{\not 0}$. **b**, Conically modulated order of the magnetic Mn^{2+} moments on the Mn1 and Mn2 positions. Bold arrows show the resulting spontaneous magnetization M_z and spontaneous polarization P_z. **c**, Like **b**, but for reversed spontaneous magnetization. **d**, Geometry of the SHG transmission experiment with light incident onto a z-cut Mn_2GeO_4 platelet. The sample is exposed to a magnetic field H_z and it is rotated around the y axis so that the optical excitation does not occur in perpendicular geometry.

Extended Data Figure 3: **SHG coupling and interference.** **a**, Spatially resolved SHG image of a z-cut Co_3TeO_6 sample. At 5 K, a magnetization-induced SHG contribution from χ_{xyy} and a crystallographically induced SHG contribution from χ_{yyy} are present. The χ_{xyy} light waves from opposite domains differ by 180° because of proportionality to the spontaneous magnetization $\pm M_{x,z}$. The phase of the χ_{yyy} wave is homogeneous across the sample because it is blind to the magnetic order. Constructive ($+M_{x,z}$) and destructive ($-M_{x,z}$) interference of the magnetic and crystallographic SHG contributions therefore yields the opposite magnetic domain states as regions of different brightness. **b**, Image of the same region as in **a** but at 30 K where $M_{x,z} = 0$ so that only the homogeneous crystallographic SHG contribution from χ_{yyy} remains. The scale bar measures 500 μm.

Extended Data Figure 4: **Inversion of ferroelectric domain pattern in a x-cut Mn_2GeO_4 sample.** Sequentially taken SHG images of $\pm P_z$ domains on a x-oriented Mn_2GeO_4 sample at given magnetic fields H_z. Note that the same domain inversion behaviour as on the z-cut sample in Fig. 4 is observed. Because of the small SHG contrast, opposite polarization domain states are highlighted by colour shading. Darker or black areas are caused by cracks and pores in the Mn_2GeO_4 sample. The scale bar measures 500 μm.

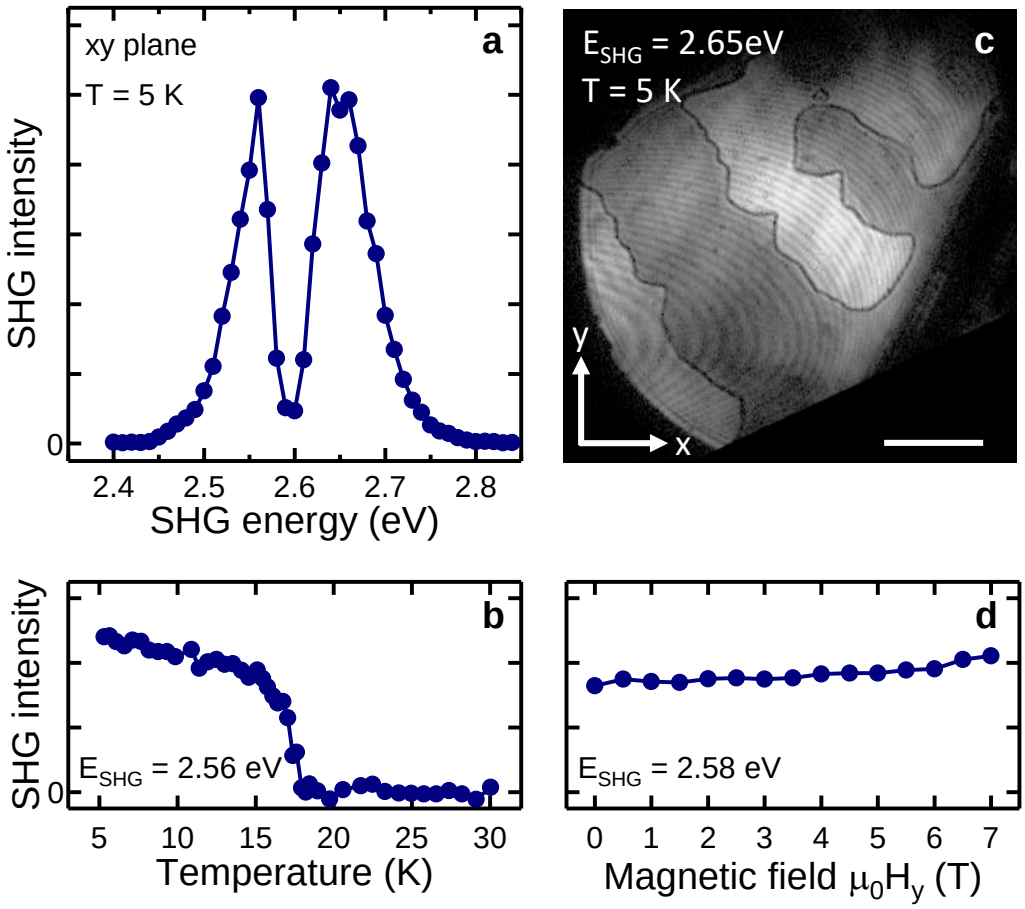
xy plane
T = 5 K
a
SHG intensity
0
2.4
2.5
2.6
2.7
2.8
SHG energy (eV)
E_SHG = 2.65eV
T = 5 K
c
y
x
b
SHG intensity
0
E_SHG = 2.56 eV
5
10
15
20
25
30
Temperature (K)
d
E_SHG = 2.58 eV
0
1
2
3
4
5
6
7
Magnetic field μ0Hy (T)

Figure 1

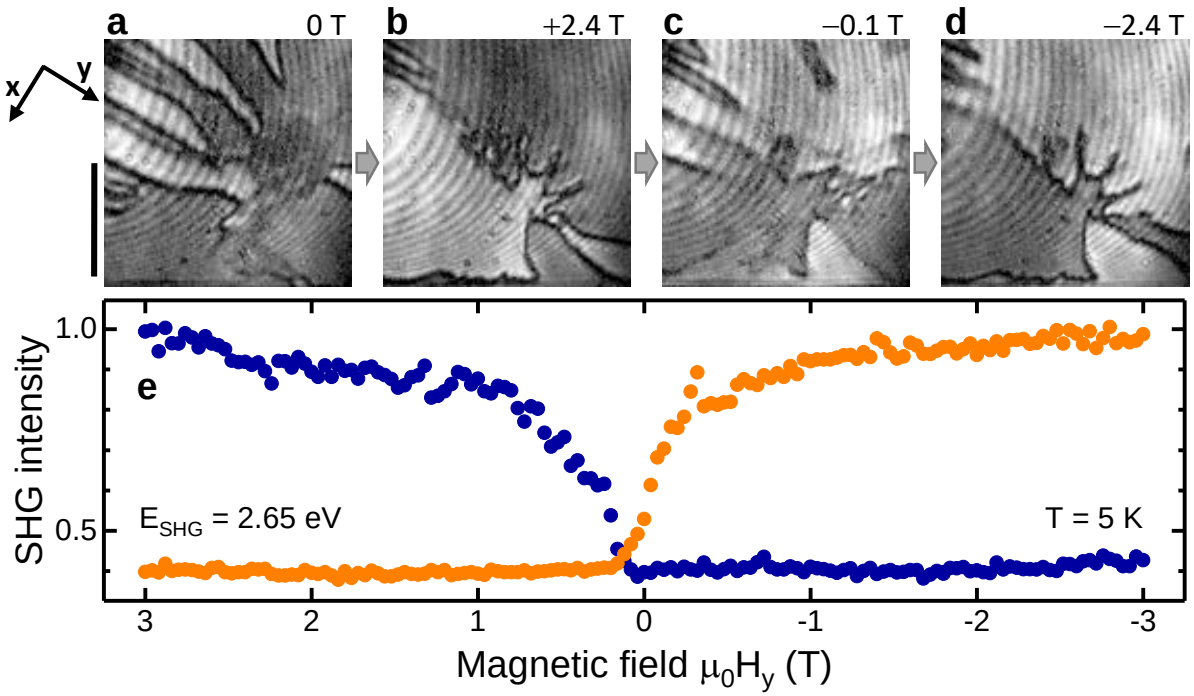
a
0 T
b
+2.4 T
c
−0.1 T
d
−2.4 T
x
y
e
SHG intensity
1.0
0.5
E_SHG = 2.65 eV
T = 5 K
3
2
1
0
-1
-2
-3
Magnetic field μ0Hy (T)

Figure 2

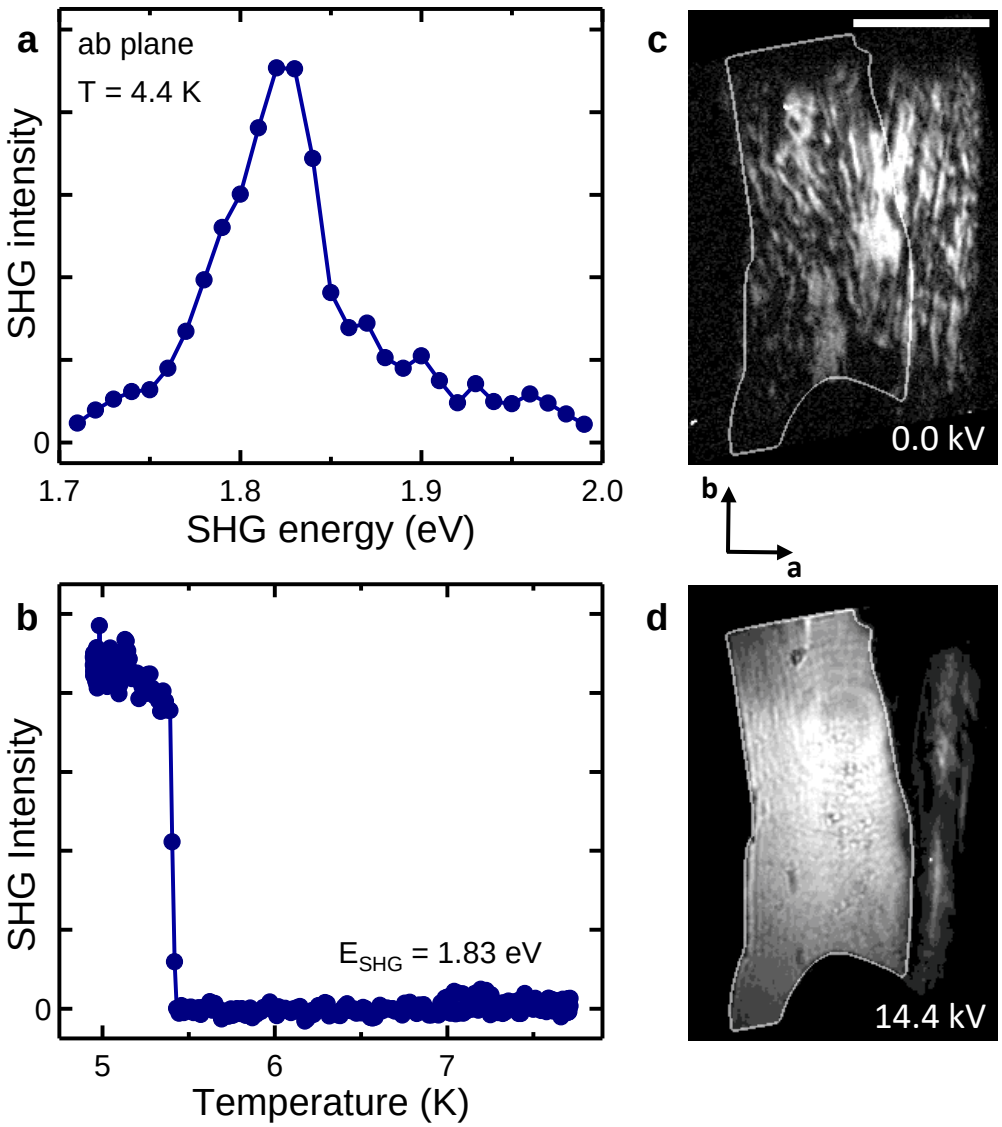
a
ab plane
T = 4.4 K
SHG intensity
0
1.7
1.8
1.9
2.0
SHG energy (eV)
b
SHG Intensity
0
5
6
7
Temperature (K)
E_SHG = 1.83 eV
c
0.0 kV
b
a
d
14.4 kV

Figure 3

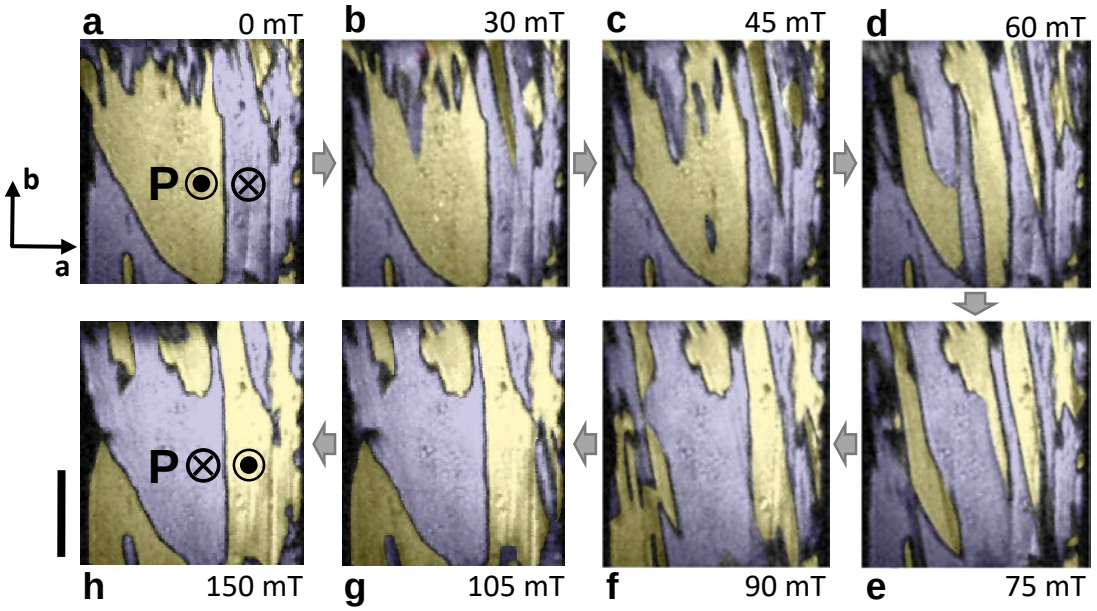

Figure 4

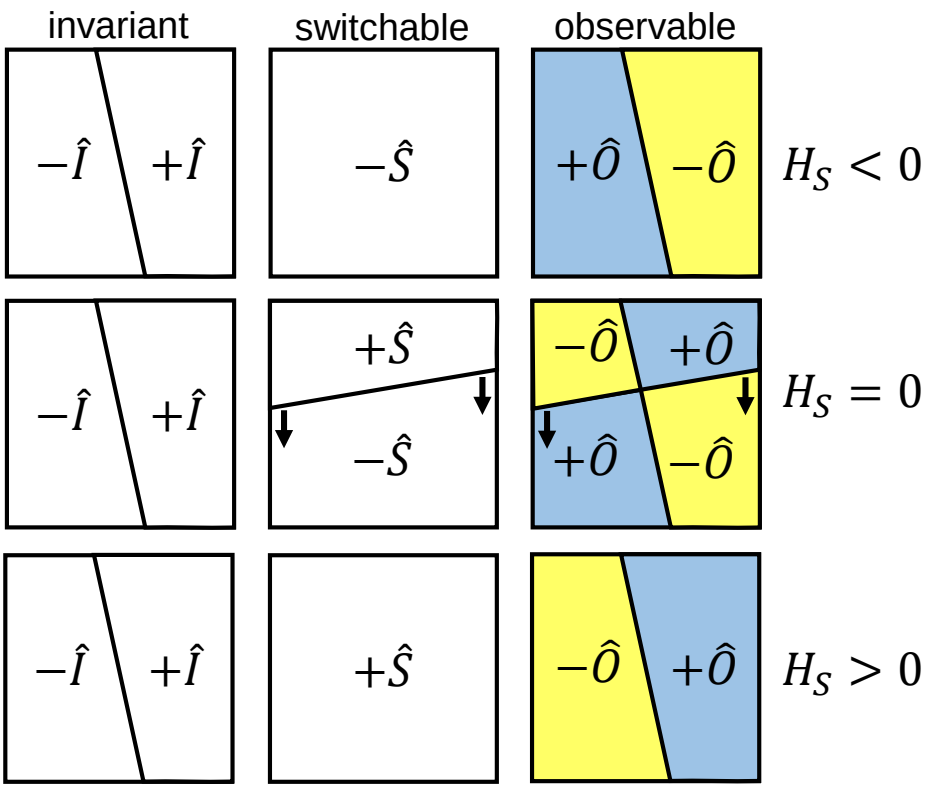
invariant
switchable
observable
$-\hat{I}$
$+\hat{I}$
$-\hat{S}$
$+\hat{O}$
$-\hat{O}$
$H_S < 0$
$+\hat{S}$
$H_S = 0$
$H_S > 0$

Figure 5